On the stability of nucleic acid feedback control systems☆

Nuno Miguel Gomes Paulino [a,*], Mathias Foo [b], Jongmin Kim [c], Declan G. Bates [a]

[a] *Warwick Integrative Synthetic Biology Centre, School of Engineering, University of Warwick, Coventry CV4 7AL, UK*
[b] *School of Mechanical, Aerospace and Automotive Engineering, Coventry University, Coventry CV1 5FB, UK*
[c] *Department of Integrative Biosciences and Biotechnology, Pohang University of Science and Technology*
(POSTECH), Pohang, Gyeongbuk, 37673, South Korea

ARTICLE INFO

ABSTRACT

Recent work has shown how chemical reaction network theory may be used to design dynamical systems that can be implemented biologically in nucleic acid-based chemistry. While this has allowed the construction of advanced open-loop circuitry based on cascaded DNA strand displacement (DSD) reactions, little progress has so far been made in developing the requisite theoretical machinery to inform the systematic design of feedback controllers in this context. Here, we develop a number of foundational theoretical results on the equilibria, stability, and dynamics of nucleic acid controllers. In particular, we show that the implementation of feedback controllers using DSD reactions introduces additional nonlinear dynamics, even in the case of purely linear designs, e.g. PI controllers. By decomposing the effects of these non-observable nonlinear dynamics, we show that, in general, the stability of the linear system design does not necessarily imply the stability of the underlying chemical reaction network, which can be lost under experimental variability when feedback interconnections are introduced. We provide an in-depth theoretical analysis, and present an example to illustrate when the linear design does not capture the instability of the full nonlinear system implemented as a DSD reaction network, and we further confirm these results using Visual DSD, a bespoke software tool for simulating nucleic acid-based circuits. Our analysis highlights the many interesting and unique characteristics of this important new class of feedback control systems.

© 2020 Elsevier Ltd. All rights reserved.

1. Introduction

Recent advances in synthetic biology have seen the incorporation of many control engineering design principles into the construction of biomolecular circuits (Blanchini, El-Samad, Giordano, & Sontag, 2018; Hancock & Ang, 2019; Siami et al., 2020). One of the current urgent needs of this field is the development of bespoke feedback control theory that can be used to systematically design synthetic controllers for biomolecular processes. A promising direction for this work is to integrate control theory with chemical reaction network (CRN) theory within the overall context of deterministic mass action kinetics (MAK) (Tóth & Érdi,

1989), which have traditionally been used to model biochemical processes (Daniel, Rubens, Sarpeshkar, & Lu, 2013; Jeong et al., 2019; Koch, Faulon, & Borkowski, 2018). Computations using MAK implementations of polynomial Ordinary Differential Equations (ODEs) make CRNs Turing universal (Bournez, Graça, & Pouly, 2017; Fages, Le Guludec, Bournez, & Pouly, 2017) and suitable for use as an abstract programming language with which to perform biomolecular computations and design synthetic circuits and controllers (Chiu, Chiang, Huang, Jiang, & Fages, 2015; Vasić, Soloveichik, & Khurshid, 2020).

For implementation, the CRN programs can be translated into DNA strand displacement (DSD) reactions (Cardelli, 2013; Soloveichik, Seelig, & Winfree, 2010) in a systematic manner (Badelt et al., 2017). Predictable mechanistic models for DNA hybridisation and the law of mass action provide nucleic acid nanocontrollers with kinetics equivalent to the regimes of the CRN (Chen et al., 2013), and a systematic pipeline for engineering dynamical systems with DSD cascades (Srinivas, Parkin, Seelig, Winfree, & Soloveichik, 2017). Programmability, versatility and biological compatibility (Chatterjee, Chen, & Seelig, 2018; Groves et al., 2016) make nucleic acids the current molecules of choice for

molecular programming (Dalchau et al., 2018) and strong candidates for implementing future computing and control applications in synthetic biology.

In the context of feedback control, however, a key challenge with employing CRNs is their inability to directly represent negative signals, since concentrations of chemical species are always positive. For example, CRNs generally can only compute a positive difference between two positive inputs, i.e. "one-sided" subtraction (Song, Garg, Mokhtar, Bui, & Reif, 2016). The use of the so-called *dual-rail representation* with nucleic acids (Oishi & Klavins, 2011) circumvents this problem by representing each signal as the difference of concentrations of two different species. Although it increases the number of required reactions, the dual-rail representation enables the computation of a two-sided subtraction with the steady state of a CRN (Zou et al., 2017). In general, it provides an Internally Positive Representation (IPR), where a positive state–space system, together with input, state and output transformations, can realise arbitrary input/output dynamics (Cacace, Farina, Germani, & Manes, 2012). We have then a systematic process to translate control theory to implementable biochemistry with synthetic DNA oligonucleotides, where DSD networks can be assembled to represent transfer functions (Chiu et al., 2015), linear feedback systems (Oishi & Klavins, 2011; Paulino, Foo, Kim, & Bates, 2019a; Yordanov et al., 2014), and nonlinear controllers (Sawlekar, Montefusco, Kulkarni, & Bates, 2016).

In all these systems, bimolecular annihilation reactions are essential, in order to ensure that species concentrations remain within the bounds of experimental feasibility. However, as noted in Paulino, Foo, Kim, and Bates (2019b), these reactions result in a nonlinear IPR, since they introduce additional internal nonlinear dynamics that are not observable in the represented input/output linear dynamics, but become important in the presence of inevitable experimental variability in the biomolecular implementations. Here, we formally characterise the effects of the nonlinear dynamics introduced through these annihilation reactions on the equilibria and the stability of closed-loop nucleic acid systems. These results provide many useful insights that can guide the design and construction of these circuits, and also highlight some of the associated technical challenges and limitations.

1.1. Notation and preliminaries

We represent the elements of vectors and matrices $\mathbf{x} = \mathbf{M}\mathbf{v}$ with $x_j = [\mathbf{M}\mathbf{v}]_j = \sum_i m_{ji}v_i$. $\mathbf{1}$ is a vector with elements 1, and $\mathbf{I}$ is the identity matrix. The element-wise product is represented with $\mathbf{x} = \mathbf{v} \circ \mathbf{u} \Rightarrow x_j = v_j u_j$. For a vector $\mathbf{v} \geq 0$, $\|\mathbf{v}\|_1 = \mathbf{1}^T\mathbf{v}$ and $\|\mathbf{v}\|_2^2 = \mathbf{1}^T (\mathbf{v} \circ \mathbf{v})$. In the system dynamics, for brevity, time dependency is implicit, i.e. $x_j \equiv x_j(t)$, $x_j^* \equiv x_j(\infty)$ represents steady state conditions, and $X_j(s)$ is the Laplace transform of x_j. $\rho\{\mathbf{M}\}$ denotes the set of the eigenvalues λ_i of the matrix $\mathbf{M}$. We represent the set of Hurwitz matrices with $\mathcal{H}$. Given the spectral abscissa $\alpha\{\mathbf{M}\} = \max_i \Re\{\lambda_i\}$, if $\mathbf{M} \in \mathcal{H}$, then $\alpha\{\mathbf{M}\} < 0$. Given the set of lower triangular matrices $\mathcal{L}$, then for $\mathbf{M} \in \mathcal{L}$ we have that $m_{ji} = 0, i > j$, and $\lambda_i\{\mathbf{M}\} = m_{ii}$. Given the set $\mathcal{I}$ of irreducible matrices (Farina & Rinaldi, 2000), if $\mathbf{M} \in \mathcal{I}$, then there is no permutation such that $\mathbf{M} \in \mathcal{L}$. Also, $\mathbf{M} \in \mathcal{L} \Rightarrow \mathbf{M} \notin \mathcal{I}$.

$\mathbb{R}_0^+$ is the positive orthant, where all the coordinates of a vector $v_j \geq 0$. $\mathbf{M} \geq 0$ means all elements $m_{ji} \geq 0$, and $\mathbf{M} \in \mathbb{R}_0^+$. The operator $\mathbf{D}\{\mathbf{v}\}$ is defined as a diagonal matrix where $d_{jj} = v_j$ and $d_{ji} = 0, j \neq i$. If $\mathbf{m}$ is the diagonal of $\mathbf{M}$, the matrix of off-diagonal elements $\mathbf{M}^{\boxslash}$ is defined as $\mathbf{M}^{\boxslash} = \mathbf{M} - \mathbf{D}\{\mathbf{m}\}$. Defining $\mathcal{M}$ as the group of Metzler matrices, if $\mathbf{M} \in \mathcal{M}$, then $\mathbf{M}^{\boxslash} \geq 0$ and if $\mathbf{M} \in \mathcal{M}, \mathcal{H}$ then $\mathbf{m} < 0$.

A CRN is composed of a set of reactions between chemical species X_j. The dynamics of the species concentrations x_j can be approximated by ODEs using the law of mass action, assuming the system is well stirred with large numbers of molecules (Tóth & Érdi, 1989). We represent a CRN and its MAK with

$$a_1 X_1 + a_2 X_2 \xrightarrow{\gamma} b X_3 \Rightarrow \dot{x}_3 = b\gamma x_1^{a_1} x_2^{a_2} \tag{1}$$
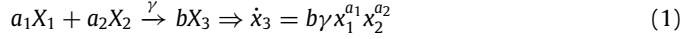
The stoichiometric coefficients a_1, a_2 and b indicate, respectively, the relative number of molecules consumed and produced during the reaction at a rate γ.

2. Dual-rail chemical representation of feedback control systems
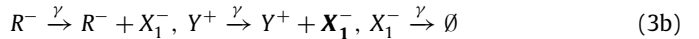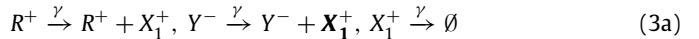
Here, we illustrate how the dual-rail representation can be used to represent the simple feedback control system shown in Fig. 1A. The overall representation considers only three types of elementary reactions,

$$\text{catalysis} : X_i \xrightarrow{\gamma} X_i + X_j \tag{2a}$$

$$\text{degradation} : X_j \xrightarrow{\gamma} \emptyset \tag{2b}$$

$$\text{annihilation} : X_i + X_j \xrightarrow{\eta} \emptyset \tag{2c}$$

The dynamics of (1) in their natural coordinates, the concentrations, results in non-negative state variables, not suitable for circuits involving negative signals such as the computation of the control error for linear feedback. To circumvent this problem, it is now a standard practice to represent both positive and negative signals with a dual-rail representation (Oishi & Klavins, 2011; Zou et al., 2017).

Definition 1. Consider two chemical species X_j^+ and X_j^-, and respective concentrations $x_j^+ \geq 0$ and $x_j^- \geq 0$. A dual-rail signal $p_j \in \mathbb{R}$ is represented by $p_j = x_j^+ - x_j^-$, with dynamics given by $\dot{p}_j = \dot{x}_j^+ - \dot{x}_j^-$.

Example 1 (*Subtraction Representation*). Let $p_1 = (r - y)$ with positive or negative outcomes $p_1, r, y \in \mathbb{R}$. With the chemical species $\{X_1^+, X_1^-, R^+, R^-, Y^+, Y^-\}$ and respective concentrations $\{x_1^+, x_1^-, r^+, r^-, y^+, y^-\}$ (M), define $r = r^+ - r^-$, $y = y^+ - y^-$, and $p_1 = x_1^+ - x_1^-$. From the following CRNs

$$R^+ \xrightarrow{\gamma} R^+ + X_1^+, \quad Y^- \xrightarrow{\gamma} Y^- + \boldsymbol{X_1^+}, \quad X_1^+ \xrightarrow{\gamma} \emptyset \tag{3a}$$

$$R^- \xrightarrow{\gamma} R^- + X_1^-, \quad Y^+ \xrightarrow{\gamma} Y^+ + \boldsymbol{X_1^-}, \quad X_1^- \xrightarrow{\gamma} \emptyset \tag{3b}$$

$$X_1^+ + X_1^- \xrightarrow{\eta} \emptyset \tag{3c}$$

we obtain the nonlinear MAK

$$\dot{x}_1^+ = -\gamma x_1^+ + \gamma r^+ + \gamma \boldsymbol{y^-} - \eta x_1^+ x_1^- \tag{4a}$$

$$\dot{x}_1^- = -\gamma x_1^- + \gamma r^- + \gamma \boldsymbol{y^+} - \eta x_1^+ x_1^- \tag{4b}$$

where the notations in bold highlight the crossed contributions from the components of y to the result p_1. Expressing the dynamics from the inputs r and y to the output p_1, under steady state conditions, we obtain the linear operation of subtraction

$$\gamma^{-1}\left(\dot{x}_1^+ - \dot{x}_1^-\right) = -x_1^+ + x_1^- + r^+ - r^- - y^+ + y^- \tag{5}$$

$$\Rightarrow \left(x_1^{+*} - x_1^{-*}\right) = \left(r^{+*} - r^{-*}\right) - \left(y^{+*} - y^{-*}\right) \tag{6}$$

$$\Rightarrow p_1^* = r^* - y^* \tag{7}$$

Since the dual-rail representation admits infinite combinations of the pair of concentrations x_1^+ and x_1^- for the same difference $p_1 = x_1^+ - x_1^-$, in practice, the annihilation reaction in (3c) is used to keep the concentrations of all molecular species low (i.e. experimentally feasible) even in the presence of transients. The cost to pay for this representation is the duplication of the catalysis and degradation reactions required. Following Oishi and
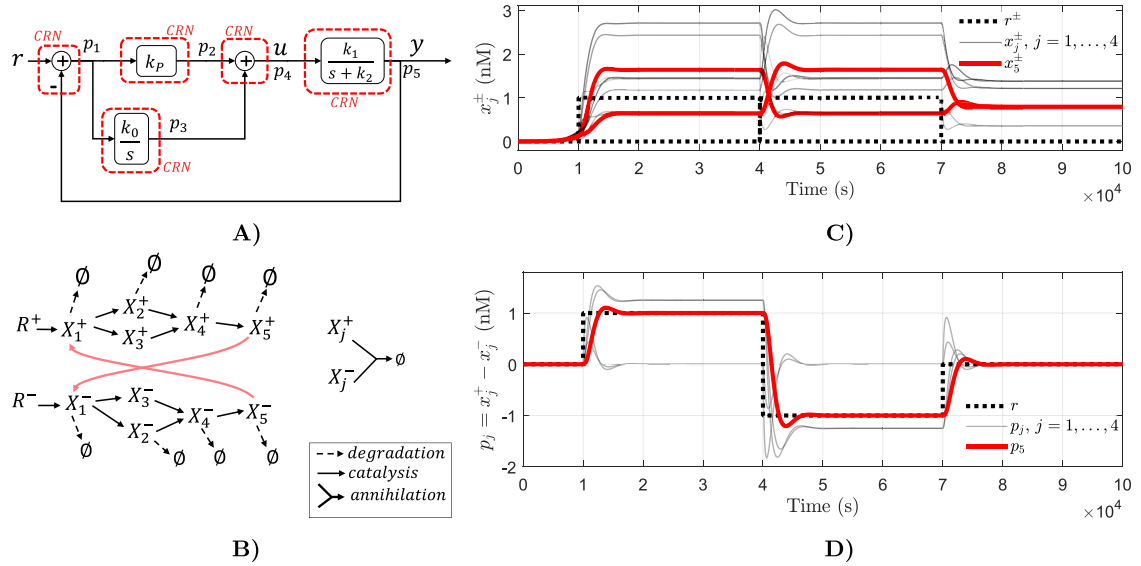
Fig. 1. Chemical representation of Example 3: (A) Frequency-domain representation of controller and plant; (B) Each signal $p_j = x_j^+ - x_j^-$ results from representing a linear operator with chemical reactions, using unimolecular catalysis and degradation reactions, and bimolecular annihilation reactions between the pairs $X_j^\pm$, resulting in a CRN where the negative feedback is introduced by the catalysis from $X_5^\mp$ to $X_1^\mp$ (in red); (C) Simulation of the MAK to a sequence of steps on the reference concentrations $r^\pm$, where $x_j^\pm \geq 0$; (D) Respective dual-rail signals, showing the reference tracking response of the output signal $y = p_5 = x_5^+ - x_5^-$ to the reference $r = r^+ - r^-$.

Klavins (2011), we compact the notation so that $X_1^\pm$ represents simultaneously both species X_1^+ and X_1^-, and $x_1^\pm$ the respective concentrations x_1^+ and x_1^-. We also abbreviate the pair of duplicated reactions $Y^+ \xrightarrow{\gamma^+} Y^+ + X_1^-$ and $Y^- \xrightarrow{\gamma^-} Y^- + X_1^+$ with $Y^\pm \xrightarrow{\gamma^\pm} Y^\pm + X_1^\mp$.

Assumption 1. The nominal parameterisation and nominal implementation assume perfectly designed reaction rates in the absence of variability, and a symmetrical parameterisation where the reaction rates are the same for each pair of duplicated reactions with $\gamma^+ = \gamma^- = \gamma$.

Assumption 1 is used in the duplicated reactions to represent linear systems (e.g., the derivation of (5) from (4)), and it is implicit in the methodology that the ideal CRNs have perfect or closely matched reaction rates, or mechanisms for fine tuning of the reaction rates (Chiu et al., 2015; Oishi & Klavins, 2011).

Definition 2. The Input–Output (I/O) system is the response $Y(s) = G(s)U(s)$, from an input $u = (u^+ - u^-)$ to an output $y = (y^+ - y^-)$. The states are also dual-rail $p_j = x_j^+ - x_j^-$, where $u, y, p_j \in \mathbb{R}$ and $u^\pm, y^\pm, x_j^\pm \in \mathbb{R}_0^+$.

Example 2 (*Plant Representation*). To chemically represent the transfer function $Y(s) = \frac{k_1}{s+k_2}U(s)$ with $u, y \in \mathbb{R}$, we take the pairs of chemical species $\{U^\pm, Y^\pm\}$ and the I/O dynamics of the CRN given by

$$U^\pm \xrightarrow{k_1} U^\pm + Y^\pm, \ Y^\pm \xrightarrow{k_2} \emptyset, \ Y^+ + Y^- \xrightarrow{\eta} \emptyset \quad (8)$$

$$\Rightarrow \dot{y}^\pm = -k_2 y^\pm + k_1 u^\pm - \eta y^+ y^- \quad (9)$$

$$\Rightarrow \dot{y}^+ - \dot{y}^- = -k_2(y^+ - y^-) + k_1(u^+ - u^-)$$

$$\Leftrightarrow \dot{y} = -k_2 y + k_1 u \quad (10)$$

Definition 2 results in linear systems because the nonlinear terms in the MAK cancel out in the ODEs of the I/O dynamics. The use of bimolecular reactions results in an IPR of a linear system based on nonlinear internal positive dynamics, in contrast to IPRs based on linear positive dynamics (Cacace et al., 2012).

Using the dual-rail CRNs to compute gains, sums, subtractions, or any proper transfer-function (Chiu et al., 2015; Oishi & Klavins, 2011), we can take a prescribed frequency-domain description of a control system, which we wish to represent chemically, and assemble a CRN representation using only the elementary reactions in (2). We now illustrate the construction of a simple example feedback system (for more complex examples see Paulino et al., 2019a; Sawlekar et al., 2016).

Example 3 (*Simple Feedback Control System*). Consider the feedback control system in Fig. 1A, which we wish to represent chemically. According to Chiu et al. (2015) and Oishi and Klavins (2011), we define the dual-rail signals $p_j = x_j^+ - x_j^-$ as the output of linear operators in the loop, each represented with reactions of the types in (2). The complete CRN in Fig. 1B gives

$$R^\pm \xrightarrow{\gamma_1^\pm} R^\pm + X_1^\pm, \ X_5^\mp \xrightarrow{\gamma_2^\mp} X_5^\mp + \boldsymbol{X_1^\pm}, \quad (11a)$$

$$X_1^\pm \xrightarrow{\gamma_3^\pm} \emptyset, \ X_1^+ + X_1^- \xrightarrow{\eta} \emptyset \quad (11b)$$

$$X_1^\pm \xrightarrow{k_0^\pm} X_1^\pm + X_3^\pm, \ X_3^+ + X_3^- \xrightarrow{\eta} \emptyset \quad (11c)$$

$$X_1^\pm \xrightarrow{\gamma_4^\pm} X_1^\pm + X_2^\pm, \ X_2^\pm \xrightarrow{\gamma_5^\pm} \emptyset, \ X_2^+ + X_2^- \xrightarrow{\eta} \emptyset \quad (11d)$$

$$X_2^\pm \xrightarrow{\gamma_6^\pm} X_2^\pm + X_4^\pm, \quad X_3^\pm \xrightarrow{\gamma_7^\pm} X_3^\pm + X_4^\pm, \quad (11e)$$

$$X_4^\pm \xrightarrow{\gamma_8^\pm} \emptyset, \quad X_4^+ + X_4^- \xrightarrow{\eta} \emptyset \quad (11f)$$

$$X_4^\pm \xrightarrow{k_1^\pm} X_4^\pm + X_5^\pm, \ X_5^\pm \xrightarrow{k_2^\pm} \emptyset, \ X_5^+ + X_5^- \xrightarrow{\eta} \emptyset \quad (11g)$$

The control error is computed in (11a)–(11b), and the integral gain is represented in (11c). The gain k_P results from the steady state conditions of (11d), where $k_P^\pm = \gamma_4^\pm/\gamma_5^\pm$, and (11e)–(11f) sum the contributions of the control inputs to the plant represented in (11g). The resulting ODEs using MAK are given by

$$\dot{x}_1^\pm = -\gamma_3^\pm x_1^\pm + \gamma_2^\mp x_5^\mp + \gamma_1^\pm r^\pm - \eta x_1^+ x_1^- \quad (12a)$$

$$\dot{x}_2^\pm = \gamma_4^\pm x_1^\pm - \gamma_5^\pm x_2^\pm - \eta x_2^+ x_2^- \quad (12b)$$

Table 1
Nominal parameters for Example 3.

$k_1^\pm = 0.0008/s$, $k_2^\pm = 0.001/s$, $k_0^\pm = 0.001/s$	
$\gamma_4^\pm = 0.0025/s$, $\gamma_{j\neq4}^\pm = 0.005/s$, $\eta = 5 \times 10^5/Ms$	

$$\dot{x}_3^\pm = k_0^\pm x_1^\pm - \eta x_3^+ x_3^- \tag{12c}$$

$$\dot{x}_4^\pm = \gamma_6^\pm x_2^\pm + \gamma_7^\pm x_3^\pm - \gamma_8^\pm x_4^\pm - \eta x_4^+ x_4^- \tag{12d}$$

$$\dot{x}_5^\pm = k_1^\pm x_4^\pm - k_2^\pm x_5^\pm - \eta x_5^+ x_5^- \tag{12e}$$

Within Assumption 1, and assuming also that $\gamma_5^\pm = \epsilon_2$, $\gamma_1^\pm = \gamma_2^\pm = \gamma_3^\pm = \epsilon_1$ and $\gamma_6^\pm = \gamma_7^\pm = \gamma_8^\pm = \epsilon_4$, we obtain the linear I/O dynamics $\dot{p}_j = \dot{x}_j^+ - \dot{x}_j^-$, where

$$\begin{bmatrix} \epsilon_1^{-1}\dot{p}_1 \\ \epsilon_2^{-1}\dot{p}_2 \\ \dot{p}_3 \\ \epsilon_4^{-1}\dot{p}_4 \\ \dot{p}_5 \end{bmatrix} = \begin{bmatrix} -1 & 0 & 0 & 0 & -1 \\ k_P & -1 & 0 & 0 & 0 \\ k_0 & 0 & 0 & 0 & 0 \\ 0 & 1 & 1 & -1 & 0 \\ 0 & 0 & 0 & k_1 & -k_2 \end{bmatrix} \begin{bmatrix} p_1 \\ p_2 \\ p_3 \\ p_4 \\ p_5 \end{bmatrix} + \begin{bmatrix} r \\ 0 \\ 0 \\ 0 \\ 0 \end{bmatrix} \tag{13}$$

The crossed contributions $X_5^\mp \xrightarrow{\gamma_2^\mp} X_5^\mp + X_1^\pm$ in (11a) result in the crossed contribution $\gamma_2^\mp x_5^\mp$ in (12a), and from $\dot{x}_1^+ - \dot{x}_1^-$ we get $p_1^* = r^* - p_5^* = r^* - y^*$. The contributions to the actuation $u = x_4^+ - x_4^-$ add up in the steady state results of (12d) and $p_4^* = p_2^* + p_3^*$ in (13).

Remark 1. The computation of the subtraction, sum and gain with CRNs are exact only at steady state. However, part of (13) can be expressed as a singular perturbation model (Kokotovic, Khalil, & O'Reilly, 1999), where by increasing ϵ_i, we get timescale separation and a quasi steady state approximation for the fast variables. The impact of the additional transient dynamics for subtraction, gain and summation can then be mitigated by setting reaction rates γ_i faster than the dynamics of the controller and plant.

For simulation of the MAK, we set the reference signal as a sequence of steps, where only one of the concentrations $r^+ > 0$ or $r^- > 0$ at any given time, with the nominal parameterisation in Table 1. For timescale separation, the rates γ_i, $i = 1 \ldots 8$ are set faster than the dynamics of the controller and plant. In Fig. 1C we have the positive dynamics in the natural coordinates $x_j^\pm$ from (12). In Fig. 1D, the I/O linear dynamics are recovered from the MAK with $p_j = x_j^+ - x_j^-$, and the linear control system's output $y = p_5$ successfully tracks the reference r. The CRN in (11) can then be systematically translated to DSD reactions. The equivalences between each elementary reaction in (2) and the sets of these DSD reactions are detailed in Section 7.

3. Dynamics of the chemical reaction network

The construction methodology in Section 2 rests on mapping ODE's to deterministic MAK, constraining the representation to the assumptions of the latter. We now define the deterministic dynamics for the class of systems analysed in this work, which includes the dual-rail representation of linear negative feedback (Oishi & Klavins, 2011; Paulino et al., 2019a; Yordanov et al., 2014). We retain the natural non-negative coordinates, where states are the concentrations $x_j^\pm$, and the input vector contains both positive and negative components for the reference $\mathbf{r} = [r^+, r^-]^T$, $r^\pm \in \mathbb{R}_0^+$.

Definition 3. Defining the state $\mathbf{x} \in \mathbb{R}_0^+$ as the vector of species concentrations, the MAK of the constructed CRN result in

$$\mathbf{x} = \left[(\mathbf{x}^+)^T \mid (\mathbf{x}^-)^T \right]^T = \left[x_1^+ \quad \ldots \quad x_N^+ \mid x_1^- \quad \ldots \quad x_N^- \right]^T \tag{14}$$

$$\Rightarrow \dot{\mathbf{x}} = \left(\mathbf{A}^\boxtimes - \mathbf{D}\{|\mathbf{a}|\} \right) \mathbf{x} + \mathbf{B}\mathbf{r} - \eta \left(\mathbf{P}\mathbf{x} \right) \circ \mathbf{x} \tag{15}$$

$$\mathbf{P} = \begin{bmatrix} \mathbf{0} & \mathbf{I} \\ \mathbf{I} & \mathbf{0} \end{bmatrix} \Rightarrow (\mathbf{P}\mathbf{x}) \circ \mathbf{x} = \begin{bmatrix} \mathbf{x}^+ \circ \mathbf{x}^- \\ \mathbf{x}^+ \circ \mathbf{x}^- \end{bmatrix} \tag{16}$$

The dynamics of the unimolecular reactions depend linearly on the state with $\mathbf{A}\mathbf{x}$, where $\mathbf{A} = \mathbf{A}^\boxtimes - \mathbf{D}\{|\mathbf{a}|\}$. By construction $\mathbf{A} \in \mathcal{M}$, since the catalysis rates end up on the off-diagonal elements $\mathbf{A}^\boxtimes \geq 0$ and the degradation rates result in non-positive elements in the diagonal of $\mathbf{D}\{\mathbf{a}\}$ ($\mathbf{a} \leq 0$). The contributions from the bimolecular reactions result in the terms $-\eta\mathbf{x}^+ \circ \mathbf{x}^-$ in (16). Furthermore, we can decompose the dynamics into non-negative and non-positive contributions where $\mathbf{D}\{\mathbf{a}\} - \eta (\mathbf{P}\mathbf{x}) \circ \mathbf{x} \leq 0$, and $\mathbf{A}^\boxtimes\mathbf{x} + \mathbf{B}\mathbf{r} \geq 0$.

Rewriting (15) according to the partition in (14) yields

$$\begin{cases} \dot{\mathbf{x}}^+ = \mathbf{A}_1^+\mathbf{x}^+ + \mathbf{A}_2^-\mathbf{x}^- + \mathbf{B}_1^+r^+ - \eta\mathbf{x}^+ \circ \mathbf{x}^- \\ \dot{\mathbf{x}}^- = \mathbf{A}_2^+\mathbf{x}^+ + \mathbf{A}_1^-\mathbf{x}^- + \mathbf{B}_1^-r^- - \eta\mathbf{x}^+ \circ \mathbf{x}^- \end{cases} \tag{17}$$

$$\Leftrightarrow \dot{\mathbf{x}}^\pm = \mathbf{A}_1^\pm\mathbf{x}^\pm + \mathbf{A}_2^\mp\mathbf{x}^\mp + \mathbf{B}_1^\pm r^\pm - \eta\mathbf{x}^+ \circ \mathbf{x}^- \tag{18}$$

and we have matrices $\mathbf{A}$ and $\mathbf{B}$ structured into

$$\mathbf{A} = \begin{bmatrix} \mathbf{A}_1^+ & \mathbf{A}_2^- \\ \mathbf{A}_2^+ & \mathbf{A}_1^- \end{bmatrix}, \quad \mathbf{B} = \begin{bmatrix} \mathbf{B}_1^+ & \mathbf{0} \\ \mathbf{0} & \mathbf{B}_1^- \end{bmatrix} \tag{19a}$$

$$\mathbf{A}_1^\pm = \left(\mathbf{A}_1^\pm \right)^\boxtimes + \mathbf{D}\{\mathbf{a}_1^\pm\}, \quad \mathbf{a}_1^\pm \leq 0, \quad \mathbf{A}_2^\pm = \left(\mathbf{A}_2^\pm \right)^\boxtimes \tag{19b}$$

From Definition 3 we have that $\mathbf{A}_j^\pm \in \mathcal{M}$ and the degradation rates are in the diagonal of $\mathbf{A}_1^\pm$. For the catalysis reaction rates, we have $\gamma : X_i^\pm \xrightarrow{\gamma} X_i^\pm + X_j^\pm, j \neq i \Rightarrow \gamma = \left[\left(\mathbf{A}_1^\pm \right)^\boxtimes \right]_{ji}$, except for the crossed catalysis representing negative signs, as in the feedback subtraction, where we have $\gamma : X_i^\pm \xrightarrow{\gamma} X_i^\pm + X_j^\mp, j \neq i \Rightarrow \gamma = \left[\mathbf{A}_2^\pm \right]_{ji}$. Because the catalysis and degradation reactions are duplicated, both matrices $\mathbf{A}_i^\pm$ retain the same structure, but not necessarily the same parameterisation (similarly for the pair $\mathbf{B}_1^\pm$). Matrices $\mathbf{A}_i^+$ and $\mathbf{B}_1^+$ are populated with the reaction rates γ_j^+, and their counterparts $\mathbf{A}_i^-$ and $\mathbf{B}_1^-$ with γ_j^-.

3.1. The dynamics in the natural coordinates are positive and non-linear

The structure of the dynamics in (15) emerges for any network built according to Section 2, and several structural properties can be derived for the class of systems in Definition 3. With $\mathbf{v} = \mathbf{B}\mathbf{r} \geq 0$, and $\mathbf{g}\{\mathbf{x}\} = -\eta (\mathbf{P}\mathbf{x})$, the following Lemma 1 shows that the nonlinear dynamics in their natural coordinates in (15) are non-negative.

Lemma 1. *For a vector function $\mathbf{g}\{\mathbf{x}\}$, if $\mathbf{M} \in \mathcal{M}$, $\mathbf{v} \geq 0$, and $\mathbf{x}(0) > 0$, the dynamics $\dot{\mathbf{x}} = \mathbf{M}\mathbf{x} + \mathbf{x} \circ \mathbf{g}\{\mathbf{x}\} + \mathbf{v}$ are non-negative.*

Proof. For each component $\dot{x}_j = [\mathbf{M}\mathbf{x}]_j + x_j[\mathbf{g}\{\mathbf{x}\}]_j + v_j$. If $x_j = 0$ and $\exists_{i\neq j} : x_i > 0$, then $\dot{x}_j = [\mathbf{M}\mathbf{x}]_j + \mathbf{v} \geq 0$ and the trajectory remains in $\mathbb{R}_0^+$. $\square$

3.2. The positive nonlinear dynamics are unobservable in the I/O dynamics of the linear representation

The construction of the CRN for the dual-rail representation in Section 2 relies on Assumption 1 to have an equivalency between the resulting I/O system of Definition 2 and a linear control system we wish to represent. The consequences of Assumption 1 on the designed dynamics (15) become clearer in the new rotated coordinates.

Definition 4. The rotated coordinates $p_j = x_j^+ - x_j^- \in \mathbb{R}$ and $q_j = x_j^+ + x_j^- \in \mathbb{R}_0^+$ result from the similarity transformation $\mathbf{W}$, where

$$\begin{bmatrix} \mathbf{p} \\ \mathbf{q} \end{bmatrix} = \begin{bmatrix} \mathbf{I} & -\mathbf{I} \\ \mathbf{I} & \mathbf{I} \end{bmatrix} \mathbf{x} = \begin{bmatrix} \mathbf{W}_p \\ \mathbf{W}_q \end{bmatrix} \mathbf{x} = \mathbf{W}\mathbf{x} \tag{20}$$

We also have that $\mathbf{W}^{-1} = \frac{1}{2}\mathbf{W}^T$, $\mathbf{W}_p\left((\mathbf{Px}) \circ \mathbf{x}\right) = 0$ and $\mathbf{W}_q\left((\mathbf{Px}) \circ \mathbf{x}\right) = 2\left(\mathbf{x}^+ \circ \mathbf{x}^-\right)$. The rotated dynamics are then given by

$$\begin{bmatrix} \dot{\mathbf{p}} \\ \dot{\mathbf{q}} \end{bmatrix} = \begin{bmatrix} \mathbf{R}_{11} & \mathbf{R}_{12} \\ \mathbf{R}_{21} & \mathbf{R}_{22} \end{bmatrix} \begin{bmatrix} \mathbf{p} \\ \mathbf{q} \end{bmatrix} + \begin{bmatrix} \mathbf{W}_p \\ \mathbf{W}_q \end{bmatrix} \mathbf{Br} \\ - \frac{\eta}{2} \begin{bmatrix} 0 \\ \mathbf{q} \circ \mathbf{q} - \mathbf{p} \circ \mathbf{p} \end{bmatrix} \tag{21}$$

Remark 2. From the structures in Definition 3 and (19) (recall that $\mathbf{a}_1^{\pm} \leq 0$), we have that

$$\mathbf{R}_{22} = \frac{\left(\mathbf{A}_1^+ + \mathbf{A}_1^- + \mathbf{A}_2^+ + \mathbf{A}_2^-\right)^{\boxtimes}}{2} - \frac{\mathbf{D}\left\{\left|\mathbf{a}_1^+\right| + \left|\mathbf{a}_1^-\right|\right\}}{2}$$

$$\mathbf{R}_{11} = \frac{\left(\mathbf{A}_1^+ + \mathbf{A}_1^- - \mathbf{A}_2^+ - \mathbf{A}_2^-\right)^{\boxtimes}}{2} - \frac{\mathbf{D}\left\{\left|\mathbf{a}_1^+\right| + \left|\mathbf{a}_1^-\right|\right\}}{2}$$

$$\mathbf{R}_{12} = \frac{\left(\mathbf{A}_1^+ - \mathbf{A}_1^- - \mathbf{A}_2^+ + \mathbf{A}_2^-\right)^{\boxtimes}}{2} - \frac{\mathbf{D}\left\{\left|\mathbf{a}_1^+\right| - \left|\mathbf{a}_1^-\right|\right\}}{2}$$

$$\mathbf{R}_{21} = \frac{\left(\mathbf{A}_1^+ - \mathbf{A}_1^- + \mathbf{A}_2^+ - \mathbf{A}_2^-\right)^{\boxtimes}}{2} - \frac{\mathbf{D}\left\{\left|\mathbf{a}_1^+\right| - \left|\mathbf{a}_1^-\right|\right\}}{2}$$

The diagonal of $\mathbf{R}_{22}$ is non-positive, given by the average of the diagonals of $\mathbf{A}_1^{\pm}$. Also $\mathbf{A}_j^{\pm} \in \mathcal{M} \Rightarrow \mathbf{R}_{22} \in \mathcal{M}$.

Definition 5. Consider the condition of perfectly identical reaction rates from Assumption 1. The nominal matrices (represented with an upper bar) are defined as $\mathbf{A}_1^{\pm} = \bar{\mathbf{A}}_1$, $\mathbf{A}_2^{\pm} = \bar{\mathbf{A}}_2$, $\mathbf{B}_1^{\pm} = \bar{\mathbf{B}}_1$.

Proposition 1. *For the nominal symmetrical parameterisation in Definition 5, the nonlinear dynamics are unobservable in the I/O system, due to the serial structure of the nominal rotated dynamics given by*

$$\dot{\mathbf{p}} = \bar{\mathbf{R}}_{11}\mathbf{p} + \mathbf{W}_p\bar{\mathbf{B}}\mathbf{r} \tag{22a}$$

$$\dot{\mathbf{q}} = \bar{\mathbf{R}}_{22}\mathbf{q} + \mathbf{W}_q\bar{\mathbf{B}}\mathbf{r} + \frac{\eta}{2}\mathbf{p} \circ \mathbf{p} - \frac{\eta}{2}\mathbf{q} \circ \mathbf{q} \tag{22b}$$

Proof. Applying Definition 5 to the matrices in Remark 2, it follows immediately that $\bar{\mathbf{R}}_{12} = \bar{\mathbf{R}}_{21} = 0$, $\bar{\mathbf{R}}_{11} = \bar{\mathbf{A}}_1 - \bar{\mathbf{A}}_2$, $\bar{\mathbf{R}}_{22} = \bar{\mathbf{A}}_1 + \bar{\mathbf{A}}_2$, and thus the serial structure of (22a)–(22b) (illustrated in Fig. 2) means that $\mathbf{p}$ evolves independently of $\mathbf{q}$, making $\mathbf{q}$ unobservable in any output of the I/O dynamics. $\square$

Noting that (22a) corresponds to the dynamics of the I/O system from Definition 2, we can use $\mathbf{W}$ to analyse the interactions between the linear I/O dynamics $\dot{\mathbf{p}}$ and the remaining internal dynamics $\dot{\mathbf{q}}$, which are nonlinear and non-negative (by Definition 4, $x_j^{\pm} \geq 0 \Rightarrow q_j \geq 0$).

Assumption 2. Assume hereafter that the dynamics we wish to represent result in stable I/O dynamics, and therefore $\bar{\mathbf{R}}_{11} \in \mathcal{H}$ and $\bar{\mathbf{R}}_{11}^{-1}$ exists.

4. Equilibria of the chemical reaction network

We now compare the equilibria of the CRN with and without feedback, to analyse how feedback changes the fundamental properties of the system.
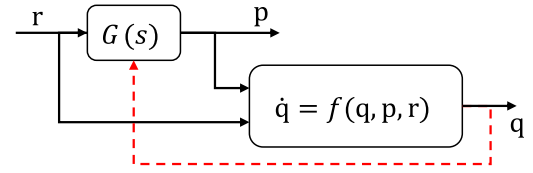

Fig. 2. Interconnection between the I/O dynamics and the underlying positive dynamics in the rotated coordinates. The dashed connection is absent with the nominal symmetric parameterisation from Definition 5.

Definition 6. We define a cascaded system as a set of DSD reactions without feedback, where the catalysis reactions do not depend directly or indirectly on the chemical species downstream.

Cascaded strand displacement reactions are well suited to systematically build large computational and logic gate circuitry (Song et al., 2016; Zou et al., 2017). The cascaded structure of the represented linear system results in a state matrix that can be permuted such that $\bar{\mathbf{R}}_{11} \in \mathcal{L}$. Under Assumptions 1 and 2, and from Remark 2, we have $\bar{\mathbf{R}}_{11} \in \mathcal{L} \Rightarrow \bar{\mathbf{A}}_1, \bar{\mathbf{A}}_2 \in \mathcal{L}$, and $\bar{\mathbf{R}}_{11} \in \mathcal{L}, \mathcal{H} \Rightarrow \bar{\mathbf{R}}_{22} \in \mathcal{L}, \mathcal{H}$. For example, representing the open loop of Fig. 1A without feedback (removing $X_5^{\pm} \to X_5^{\pm} + X_1^{\mp}$ in Fig. 1B) results in a cascade of serial and parallel unimolecular reactions. In this particular case, it also results in $\bar{\mathbf{A}}_2 = 0$, but in general, we can have $\bar{\mathbf{A}}_2 \geq 0$ if there are subtractions in the cascaded I/O dynamics. The feedback reactions $X_5^{\pm} \to X_5^{\pm} + X_1^{\mp}$ connect the output to the input of the cascade, and mass is transferred back into the input of the cascade. Including feedback in the I/O dynamics leads to feedback within the network, and the cascaded structure is lost.

Due to the triangular structure, the equilibrium of the unforced dynamics can be easily computed sequentially for each coordinate to show that there is a unique equilibrium at $\mathbf{q} = 0$ for the cascaded systems. In the presence of feedback this is no longer possible since the states will depend on the output, and it follows that $\exists_{i>j} : \left[\bar{\mathbf{R}}_{11}\right]_{ji} > 0$. Consequently, all the states involved in the closed loop become interdependent, and $\bar{\mathbf{R}}_{11}$ cannot be a lower triangular matrix.

Remark 3. The interdependent evolution of all the states is reflected in the irreducibility of the state matrix $\bar{\mathbf{R}}_{22}$. If $\bar{\mathbf{R}}_{22} \in \mathcal{I}, \mathcal{M}$, for each coordinate j, $\exists_{i \neq j} : \left[\bar{\mathbf{R}}_{22}\right]_{ji} > 0$. Therefore the trajectory of q_j always depends on another coordinate q_i, making the network irreducible.

Proposition 2. *Consider $\mathbf{M} \in \mathcal{I}, \mathcal{M}$ such that $\mathbf{M} = \mathbf{M}^{\boxtimes} + \mathbf{D}\{\mathbf{m}\}$, $\mathbf{m} \leq 0$, a scalar $k > 0$, and the dynamics $\dot{\mathbf{q}} = \mathbf{M}\mathbf{q} - k\mathbf{q} \circ \mathbf{q}$ with equilibrium $\mathbf{q}^*$. Then we have the following: (i) $\exists_j q_j^* = 0 \Rightarrow q_{i \neq j}^* = 0$; (ii) the unforced dynamics may admit a second positive equilibrium $\mathbf{q}^* > 0$, proportional to k^{-1}.*

Proof. From the equilibrium condition for each coordinate j we take the non-negative roots

$$kq_j^2 + |m_{jj}|q_j - \sum_{i \neq j} m_{ji}q_i = 0 \tag{23}$$

$$\Rightarrow q_j = \frac{1}{2k}\left(-|m_{jj}| + \sqrt{m_{jj}^2 + 4k\sum_{i \neq j} m_{ji}q_i}\right) \geq 0 \tag{24}$$

(i) If $\sum_{i \neq j} m_{ji}q_i = 0$, then $q_j = 0$, and we disregard the negative solution $q_j = -|m_{jj}|/k$. Since $\mathbf{M} \in \mathcal{I}$, for every coordinate j, $\exists_{l \neq j} : m_{jl} > 0$, and $q_j = 0 \Leftrightarrow q_l = 0$. We also have that for any

$i \neq j : m_{ij} > 0$, $q_i = 0 \Leftrightarrow q_j = 0$. Hence, if $q_j = 0 \Rightarrow \forall_{i \neq j}$, $q_i = 0$, and we cannot have an equilibrium where only some of the states are at zero.

(ii) If $\exists_{i \neq j} : m_{ji} > 0$ and the coordinate i is at a positive equilibrium $q^*_{i \neq j} > 0$, then $\sum_{i \neq j} m_{ji} q^*_i > 0$. The non-negative roots for each coordinate j result from solving the system (24). Note that even if $m_{jj} = 0$, then $q^*_j > 0$. Combining **(i)** and **(ii)**, if $\mathbf{M} \in \mathcal{I}$, the system may have a positive equilibrium $\mathbf{q}^* > 0$, which can be scaled down with k, since $\lim_{k \to \infty} q^*_j = 0$. $\square$

Example 4. Consider the CRN representation of a linear system with a single input u and negative feedback between its states x and y ($c_2 > 0$)

$$\dot{x} = -d_1 x - c_2 y + u, \quad \dot{y} = -d_2 y + c_1 x \tag{25}$$

with the CRN representation given by

$$\begin{cases} U^\pm \xrightarrow{1} U^\pm + X^\pm, \ X^\pm \xrightarrow{d_1} \emptyset, \ X^+ + X^- \xrightarrow{k} \emptyset \\ X^\pm \xrightarrow{c_1} X^\pm + Y^\pm, \ Y^\pm \xrightarrow{d_2} \emptyset, \ Y^+ + Y^- \xrightarrow{k} \emptyset \\ \qquad Y^\pm \xrightarrow{c_2} Y^\pm + X^\mp, \ U^+ + U^- \xrightarrow{k} \emptyset \end{cases} \tag{26}$$

$$\Rightarrow \bar{\mathbf{R}}_{11} = \begin{bmatrix} -d_1 & -c_2 \\ c_1 & -d_2 \end{bmatrix}, \quad \bar{\mathbf{R}}_{22} = \begin{bmatrix} -d_1 & c_2 \\ c_1 & -d_2 \end{bmatrix} \tag{27}$$

Without feedback, $c_2 = 0$, then the system simplifies to a reducible serial cascade where $\bar{\mathbf{R}}_{11} = \bar{\mathbf{R}}_{22} = \bar{\mathbf{A}}_1 \in \mathcal{L}$, and the unforced dynamics $\dot{\mathbf{q}} = \bar{\mathbf{R}}_{22}\mathbf{q} - k\mathbf{q} \circ \mathbf{q}$ have a single non-negative equilibrium at $\mathbf{q} = 0$. With feedback, $c_2 > 0$ and we can replace $q_2 = c_2^{-1}(kq_1 + d_1)q_1$ in the equilibrium conditions for q_1 and obtain the polynomial

$$k^3 q_1^4 + 2k^2 d_1 q_1^3 + \left(d_1^2 + c_2 d_2 \right) k q_1^2 \\ + c_2 \left(d_2 d_1 - c_2 c_1 \right) q_1 = 0 \tag{28}$$

Using Descartes' rule of signs, if $c_2 > d_2 d_1 c_1^{-1}$, we have one positive root and the equilibrium $q^*_1 > 0$ exists.

Remark 4. Note that the use of $\bar{\mathbf{A}}_2$ to represent negative feedback in the I/O dynamics in (22a) with $\bar{\mathbf{R}}_{11} = \bar{\mathbf{A}}_1 - \bar{\mathbf{A}}_2$, results in positive feedback in the nonlinear dynamics in (22b) with $\bar{\mathbf{R}}_{22} = \bar{\mathbf{A}}_1 + \bar{\mathbf{A}}_2$

In (27) of Example 4, c_2 impacts the spectral radius of $\bar{\mathbf{R}}_{11}$ and $\bar{\mathbf{R}}_{22}$ differently. From their characteristic polynomials, we have stable I/O dynamics ($\bar{\mathbf{R}}_{11} \in \mathcal{H}$) for any $c_2 > 0$, but for a sufficiently high gain $c_2 > d_2 d_1 c_1^{-1}$, we get $\bar{\mathbf{R}}_{22} \notin \mathcal{H}$. Not coincidentally, it is the same domain for which $\mathbf{q}^* > 0$ exists.

Remark 5. The existence of positive equilibrium conditions for linear feedback systems has direct consequences for the experimental construction of these circuits. Operating at an equilibrium corresponding to high concentrations aggravates leaky reactions, where undesired triggering of strand displacement leads to unwanted outputs in the absence of inputs. Furthermore, if $\mathbf{q}^* \geq 0$ with input $\mathbf{r} = 0$, then the reactions persist even if the I/O dynamics are at rest $\mathbf{p} = 0$, leading to unnecessary, irreversible, and costly consumption of fuel species. This is in direct contrast to cascaded systems, where without input to the I/O dynamics, the CRN is at equilibrium at $\mathbf{x} = 0$, and no reactions occur.

5. Stability

We begin by proving the following lemma, which is applicable to the unforced dynamics of (15) and (22b).

Lemma 2. If $\mathbf{M} \in \mathcal{M}, \mathcal{H}$, and $\mathbf{g}\{\mathbf{x}\} < 0$ for $\mathbf{x} > 0$, then the system $\dot{\mathbf{x}} = \mathbf{M}\mathbf{x} + \mathbf{x} \circ \mathbf{g}\{\mathbf{x}\}$ is globally asymptotically stable (GAS) at $\mathbf{x} = 0$.
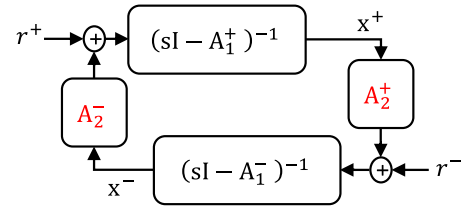

Fig. 3. Representing negative feedback with $\mathbf{A}_2^\pm \geq 0$, introduces positive feedback between positive dynamics $\mathbf{A}_1^\pm \in \mathcal{M}$.

Proof. From the stability of Metzler matrices (Farina & Rinaldi, 2000), $\mathbf{M} \in \mathcal{M}, \mathcal{H} \Rightarrow \exists_{\mathbf{d} > 0} : \mathbf{M}^T \mathbf{D}\{\mathbf{d}\} + \mathbf{D}\{\mathbf{d}\}\mathbf{M} = -\mathbf{I}$. We take the Lyapunov function $V_d\{\mathbf{x}\} = \mathbf{x}^T \mathbf{D}\{\mathbf{d}\}\mathbf{x} > 0$, and since $\mathbf{D}\{\mathbf{d}\}(\mathbf{x} \circ \mathbf{g}\{\mathbf{x}\}) = \mathbf{d} \circ \mathbf{x} \circ \mathbf{g}\{\mathbf{x}\} < 0, \forall_{\mathbf{x} > 0}$, we have that $\dot{V}_d(\mathbf{x}) = -\mathbf{I} + 2\mathbf{g}\{\mathbf{x}\}^T (\mathbf{d} \circ \mathbf{x} \circ \mathbf{x}) < 0$ $\square$

With $\mathbf{g}\{\mathbf{x}\} = -\mathbf{P}\mathbf{x}$, Lemma 2 ensures that if the network of catalysis and degradation reactions is stable, $\mathbf{A} \in \mathcal{H}$, the bimolecular reactions cannot destabilise (15). A stable CRN with $\mathbf{A} \in \mathcal{H}$ can occur if the degradation of each species is faster than their overall production, and $\mathbf{A}$ has a dominant diagonal. However, this is not the general case. The dynamics without the bimolecular reactions result in the positive feedback loop between two positive systems (see Fig. 3). Since we cannot stabilise the non-negative dynamics $\mathbf{A}_1^\pm \in \mathcal{M}$ with non-negative matrices $\mathbf{A}_2^\pm \geq 0$ (De Leenheer & Aeyels, 2001; Roszak & Davison, 2009), it is sufficient to have $\mathbf{A}_1^\pm \notin \mathcal{H}$ to give $\mathbf{A} \notin \mathcal{H}$. Even for the nominal symmetrical parameterisation, the representation has modes that are not present in the original linear system $\rho\{\bar{\mathbf{R}}\} = \rho\{\bar{\mathbf{R}}_{11}\} \cup \rho\{\bar{\mathbf{R}}_{22}\}$. While this is a problem for IPR with linear positive systems (Cacace et al., 2012), the presence of the bimolecular reactions are sometimes sufficient for stabilisation, even if $\bar{\mathbf{R}}_{22} \notin \mathcal{H}$.

5.1. The I/O dynamics determine the stability for the nominal symmetrical case

While at first glance it seems precarious to have unobservable nonlinear dynamics, for the designed nominal symmetrical case in Definition 5, it is possible to provide guarantees for stability and boundedness.

Proposition 3. The cascaded systems from Definition 6 representing stable I/O dynamics, have GAS unforced nonlinear dynamics, for $\mathbf{x} > 0$.

Proof. From Remark 2, in cascaded systems $\bar{\mathbf{R}}_{11}, \bar{\mathbf{R}}_{22} \in \mathcal{L}$, and $\rho\{\bar{\mathbf{R}}_{11}\} = \rho\{\bar{\mathbf{R}}_{22}\}$. If the I/O system is stable, then $\alpha\{\bar{\mathbf{R}}_{11}\} = \alpha\{\bar{\mathbf{R}}_{22}\} < 0$ and Lemma 2 ensures $\dot{\mathbf{q}} = \bar{\mathbf{R}}_{22}\mathbf{q} - \frac{\eta}{2}\mathbf{q} \circ \mathbf{q}$ is GAS at $\mathbf{q} = 0$. $\square$

Remark 6. We can apply Proposition 3 to the representation of individual linear operations, which by themselves are cascaded reactions. It results directly that the CRNs for summation, gain, and subtraction by themselves, have GAS unforced dynamics, and are bounded for bounded inputs. More importantly, applying it to CRNs assembled from cascading those linear operations, results in a single stable equilibrium for the complete circuit.

With the introduction of feedback, we lose the cascaded structure and create an irreducible system, even for the representation of stable I/O linear dynamics ($\bar{\mathbf{R}}_{11} \in \mathcal{H}$). If feedback leads to $\bar{\mathbf{R}}_{22} \notin \mathcal{H}$, then the following lemma states that unforced trajectories diverge away from the origin due to a diverging mode of $\bar{\mathbf{R}}_{22}$.

Lemma 3. *For the dynamics $\dot{\mathbf{q}} = \mathbf{Mq} - k\mathbf{q} \circ \mathbf{q}$, with a scalar $k > 0$, and $\mathbf{M} \in \mathcal{M}, \mathcal{I}$ but $\mathbf{M} \notin \mathcal{H}$, the equilibrium at the origin $\mathbf{q} = 0$ is unstable.*

Proof. From applying the Frobenius–Perron theorem to Metzler matrices (Farina & Rinaldi, 2000), $\mathbf{M} \in \mathcal{M}, \mathcal{I} \Rightarrow \exists_{\mathbf{w}_F > 0} : \mathbf{w}_F^T \mathbf{M} = \lambda_F \mathbf{w}_F^T$ and $\lambda_F = \alpha\{\mathbf{M}\}$. Defining the Lyapunov function $V_F(\mathbf{q}) = \mathbf{w}_F^T \mathbf{q}$, we have that $\mathbf{q} > 0 \Rightarrow V_F(\mathbf{q}) > 0$ and $\dot{V}_F(\mathbf{q}) = \mathbf{w}_F^T \dot{\mathbf{q}} = \mathbf{w}_F^T (\mathbf{q} \circ (\lambda_F \mathbf{1} - k\mathbf{q}))$. Since $\mathbf{M} \notin \mathcal{H} \Rightarrow \lambda_F > 0$, hence $\forall_j, q_j < \frac{\lambda_F}{k}$ gives that $\dot{V}_F\{\mathbf{q}\} > 0$, and the system is divergent close to the origin. $\square$

The IPR of a stable system using only linear positive systems is therefore not guaranteed to be stable (Cacace et al., 2012). However, for the nonlinear positive dynamics (22), we can still ensure boundedness with the following result.

Lemma 4. *For $\mathbf{M} \in \mathcal{M}$, $\mathbf{q}(0) > 0$, and a bounded input $\mathbf{v} \geq 0$, if $\mathbf{g}\{\mathbf{q}\} \leq -k\mathbf{q}$ (scalar $k > 0$) then the non-negative trajectories of $\dot{\mathbf{q}} = \mathbf{Mq} + \mathbf{q} \circ \mathbf{g}\{\mathbf{q}\} + \mathbf{v}$ are bounded by $\|\mathbf{q}\|_2 < k^{-1}\left(\sqrt{N}\|\mathbf{M}\|_2 + \|\mathbf{v}\|_1\|\mathbf{q}\|_2^{-1}\right)$.*

Proof. Lemma 1 guarantees that the trajectories are non-negative for $\mathbf{q}(0) > 0$. If $\mathbf{M} \in \mathcal{H}$, Lemma 2 guarantees that the system is asymptotically stable in $\mathbb{R}_0^+$ with equilibrium at $\mathbf{q} = 0$. If $\mathbf{M} \notin \mathcal{H}$, we can still show boundedness, using the linear Lyapunov function $V_1\{\mathbf{q}\} = \mathbf{1}^T\mathbf{q} = \sum_j q_j > 0$, in the domain $\mathbf{q} > 0$. We then have

$$\begin{aligned}
\dot{V}_1\{\mathbf{q}\} &= \mathbf{1}^T\mathbf{Mq} + \mathbf{1}^T\mathbf{v} + \mathbf{1}^T\mathbf{D}\{\mathbf{q}\}\mathbf{g}\{\mathbf{q}\} \\
&= \mathbf{1}^T\mathbf{Mq} + \|\mathbf{v}\|_1 + \mathbf{q}^T\mathbf{g}\{\mathbf{q}\} \\
&\leq \|\mathbf{Mq}\|_1 + \|\mathbf{v}\|_1 - k\mathbf{q}^T\mathbf{q} \\
&\leq \sqrt{N}\|\mathbf{M}\|_2\|\mathbf{q}\|_2 + \|\mathbf{v}\|_1 - k\|\mathbf{q}\|_2^2
\end{aligned}$$

We can always find large enough values of $\mathbf{q}$ such that $\|\mathbf{q}\|_2 > \frac{\sqrt{N}}{k}\|\mathbf{M}\|_2 + \frac{1}{k}\frac{\|\mathbf{v}\|_1}{\|\mathbf{q}\|_2}$ where we have $\dot{V}_1\{\mathbf{q}\} < 0$. $\square$

Applying Lemma 4 with $\mathbf{g}\{\mathbf{q}\} = -\frac{\eta}{2}\mathbf{q}$ to the unforced dynamics in (22b) we have $\|\mathbf{q}\|_2 < 2\eta^{-1}\sqrt{N}\|\bar{\mathbf{R}}_{22}\|_2$. In general, Lemma 4 is not applicable to the nonlinear dynamics (15), due to the matrix $\mathbf{P}$.

Proposition 4. *Consider the nominal dynamics in (22a)–(22b), with the symmetrical parameterisation from Assumption 1. Under Assumption 2, the I/O dynamics (22a) are stable, and the concentrations in the complete CRN are bounded and can be scaled down with a faster annihilation reaction rate η.*

Proof. Assumption 2 ensures the trajectories of $\mathbf{p}$ are bounded. We can treat $\mathbf{p}$ as an additional input to the system (22b) and apply Lemma 4 with $\mathbf{v} = \mathbf{W}_q\bar{\mathbf{B}}\mathbf{r} + \frac{\eta}{2}\mathbf{p} \circ \mathbf{p}$. The unobserved dynamics are then bounded for bounded inputs $\mathbf{r}, \mathbf{p} > 0$, and are scaled down by increasing η. $\square$

The same feedback responsible for a stable I/O linear dynamics can result in $\bar{\mathbf{R}}_{22} \notin \mathcal{H}$ (see Remark 4). Designing feedback to ensure that $\bar{\mathbf{R}}_{11}, \bar{\mathbf{R}}_{22} \in \mathcal{H}$ is impractical since it would put constraints on which I/O systems could be represented. It is one of the challenges of representing stable linear systems relying only on linear positive systems (Cacace et al., 2012), where we would need $\bar{\mathbf{A}} \in \mathcal{H}$ for the IPR to be stable. Lemma 4 lifts this constraint, albeit at the cost of a positive equilibrium.

Remark 7. With the introduction of feedback, the concentrations involved in the irreducible parts of the CRN will have positive

equilibria, and $\exists_j q_j(t) > 0$ even if $\mathbf{r} = 0$ and the I/O dynamics are stable $\alpha\{\bar{\mathbf{R}}_{11}\} < 0$. In experimental practice, this result motivates setting the annihilation rate η as high as possible, to minimise the concentrations in the circuit during operation or at equilibrium.

Remark 8. With $\bar{\mathbf{A}}_1 \in \mathcal{M}$ but $\bar{\mathbf{A}}_1 \notin \mathcal{H}$, there is no $\bar{\mathbf{A}}_2 \geq 0$ such that $\bar{\mathbf{A}}_1 + \bar{\mathbf{A}}_2 \in \mathcal{H}$ (De Leenheer & Aeyels, 2001; Roszak & Davison, 2009). Starting from a marginally stable state matrix $\alpha\{\bar{\mathbf{A}}_1\} = 0$, the introduction of feedback leads to $\alpha\{\bar{\mathbf{R}}_{22}\} \geq 0$. This raises an interesting tradeoff, where the controllers that introduce integrators in the loop transfer function (*e.g.* PI controller) lead to a positive equilibrium, which is inconvenient for implementation.

6. Stability with asymmetrical parameterisation resulting from experimental variability

The construction of the I/O dynamics in (22a) assumes the symmetrical parameterisation in Definition 5, and we have shown some of the properties intrinsic to the design methods, like positive equilibria and internal stability conditions. A parametric scattering of the $\bar{\mathbf{R}}_{11}$ in (22a) is still within Assumption 1, and as long as the I/O linear dynamics are stable $\bar{\mathbf{R}}_{11} \in \mathcal{H}$, Proposition 4 guarantees that the nonlinear dynamics are bounded.

However, when verifying the implementation of the CRN, we must account for experimental error and granularity in the affinities (Zhang et al., 2018), and analyse robustness to variations in all the reaction rates (Paulino et al., 2019b). Once we (realistically) allow the reaction rates in the CRN to vary independently, we get an asymmetric parameterisation that deviates from Assumption 1. The consequences of this asymmetry are clarified in the rotated coordinates: although the I/O dynamics $\dot{\mathbf{p}}$ are still linear in (21) ($\mathbf{W}_p(\mathbf{Px} \circ \mathbf{x}) = 0$), they depend on the nonlinear dynamics through the term $\mathbf{R}_{12}\mathbf{q}$ (absent in (22a)), with

$$\dot{\mathbf{p}} = \mathbf{R}_{11}\mathbf{p} + \mathbf{W}_p\bar{\mathbf{B}}\mathbf{r} + \mathbf{R}_{12}\mathbf{q} \tag{29}$$

Remark 9. With experimental variability, we lose the serial structure from (22). A stable I/O dynamics $\mathbf{R}_{11} \in \mathcal{H}$ no longer provides guarantees of boundedness, since it ignores the feedback between the I/O linear dynamics and the underlying nonlinear dynamics (dashed connection in Fig. 2). Therefore, we need to analyse the stability of the complete nonlinear dynamics of (15).

We investigate the stability of the nonlinear system using Lyapunov's indirect method, and the eigenvalues of the linearisation at the equilibrium of the system. For an equilibrium $\mathbf{x}^* > 0$, $\mathbf{r} = 0$, and $\mathbf{J}\{\mathbf{x}^*\} = -\mathbf{D}\{\mathbf{Px}^*\} - \mathbf{D}\{\mathbf{x}^*\}\mathbf{P}$, the linearisation of (15) results in

$$\dot{\mathbf{s}} = (\mathbf{A} + \eta\mathbf{J}\{\mathbf{x}^*\})\mathbf{s} + \mathbf{Br}_e = \mathbf{A}_s\mathbf{s} + \mathbf{Br}_e \tag{30}$$

If $\alpha\{\mathbf{A}_s\} < 0$ then the system is locally exponentially stable around the equilibrium (Khalil, 2015). The equilibrium $\mathbf{x}^* = 0$ is stable if and only if $\mathbf{A} \in \mathcal{H}$, which is in agreement with Lemma 2. With the participation of $\mathbf{J}\{\mathbf{x}^*\}$, even if $\mathbf{A} \notin \mathcal{H}$, the linearisation can still be stable around the equilibrium $\mathbf{x}^* > 0$, showing the stabilising role of the bimolecular reactions. It is also noteworthy that $\mathbf{W}_p\mathbf{J}\{\mathbf{x}^*\} = 0$, hence $\alpha\{\mathbf{R}_{11}\}$ and the stability of the linear I/O dynamics does not depend on the equilibrium.

6.1. Stability analysis of an example nucleic acid feedback control system

We now illustrate the above results for the simplest feedback control system configuration in Example 3. With the nominal parameters in Table 1, we have in Table 2 that $\bar{\mathbf{R}}_{22} \notin \mathcal{H}$, and the origin is unstable (Lemma 3). This is confirmed in Fig. 1C,

Table 2

Poles with maximum real part, for the I/O and linearised dynamics, for the nominal and asymmetrical parametrisations.

Matrix $\mathbf{M}$	Poles corresponding to $\alpha\{\mathbf{M}\}$	Stability
$\bar{\mathbf{R}}_{11}$	$(-6.3741 \pm i8.0364) \times 10^{-4}$	$\bar{\mathbf{R}}_{11} \in \mathcal{H}$
$\bar{\mathbf{R}}_{22}$	$+5.2991 \times 10^{-4}$	$\bar{\mathbf{R}}_{22} \notin \mathcal{H}$
$\bar{\mathbf{A}}_s$	-5.1614×10^{-4}	$\bar{\mathbf{A}}_s \in \mathcal{H}$
$\mathbf{R}_{11}$	$(-0.21874 \pm i15.031) \times 10^{-4}$	$\mathbf{R}_{11} \in \mathcal{H}$
$\mathbf{A}_s$	$(+0.27197 \pm 15.325i) \times 10^{-4}$	$\mathbf{A}_s \notin \mathcal{H}$

Table 3

An asymmetrical parameterisation of Example 3 which results in unstable dynamics of the CRN.

$k_1^{\pm} = 0.001064/\text{s}, \ k_2^{\pm} = 0.00067/\text{s}, \ k_0^{\pm} = 0.00133/\text{s},$
$\gamma_4^{\pm} = 0.001675/\text{s}, \ \gamma_5^{\pm} = 0.00665/\text{s} \ (k_P^{\pm} = 0.25188)$
$\gamma_1^{\pm} = \gamma_2^{\pm} = \gamma_3^- = 0.00665/\text{s}, \ \gamma_3^+ = 0.00335/\text{s}$
$\gamma_6^- = \gamma_7^{\pm} = \gamma_8^- = 0.00665/\text{s}, \ \gamma_6^+ = \gamma_8^+ = 0.00335/\text{s}$
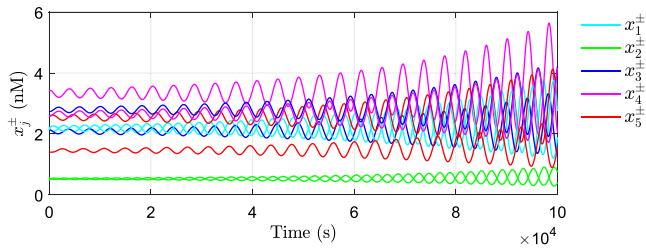$\eta = 5 \times 10^5/\text{M/s}$

Fig. 4. Trajectories of the concentrations $x_j^{\pm}$ for the MAK parameterised with the rates from Table 3 ($\mathbf{r} = 0$).
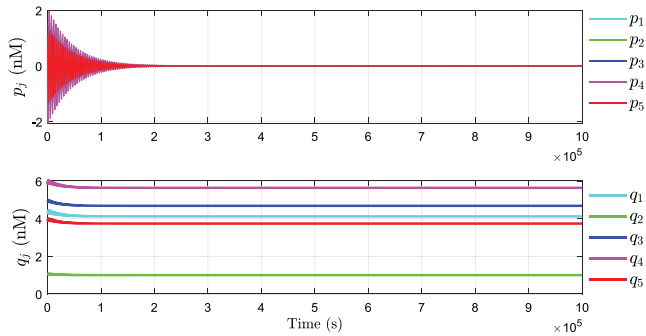

Fig. 5. Simulation of the rotated dynamics of $\dot{\mathbf{p}}$ and $\dot{\mathbf{q}}$ with decoupled matrix $\mathbf{R}$ where $\mathbf{R}_{21} = \mathbf{R}_{12} = 0$, for the parameters in Table 3.

where at $t > 7 \times 10^4$ s the reference returns to $r^{\pm} = 0$ and the state converges to a positive equilibrium $\bar{\mathbf{x}}^{+*} = \bar{\mathbf{x}}^{-*} > 0$. Table 2 shows that the nominal I/O dynamics $\bar{\mathbf{R}}_{11} \in \mathcal{H}$ and the linearisation around the nominal equilibrium $\bar{\mathbf{A}}_s \in \mathcal{H}$.
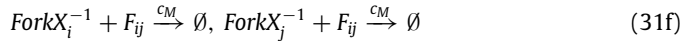
Considering experimental variability in the reaction rates leads to asymmetric parameterisations, and the stability of I/O dynamics does not guarantee stability of the CRN. To account for realistic levels of experimental variability, we introduce an uncertainty of $\pm 33\%$ in the reaction rates, which includes the asymmetrical parameterisation from Table 3. This level of variability reflects what should be achievable experimentally, since models based on toehold sequence can predict hybridisation rates within factors of 2 and 3, and the uncertainty can be further reduced with experimental parameter fitting and iterative designs of toeholds and auxiliary species concentrations (Srinivas et al., 2017; Zhang et al., 2018).

Perturbing the unforced nonlinear dynamics for this case around its equilibrium ($\mathbf{x}^* > 0$, $\mathbf{r} = 0$), results in the unstable

response of Fig. 4. The poles in Table 2 show that the linearisation with the asymmetrical parameterisation $\mathbf{A}_s$ captures the instability in a pair of conjugated poles on the right-half plane, despite the stability of the I/O linear system $\mathbf{R}_{11} \in \mathcal{H}$. Indeed, integrating the rotated dynamics with a decoupled matrix $\mathbf{R}$, where we force $\mathbf{R}_{21} = \mathbf{R}_{12} = 0$, we obtain the response of Fig. 5, where both $\mathbf{p}$ and $\mathbf{q}$ have bounded trajectories. This shows that the source of the instability of the complete nonlinear system is neither $\dot{\mathbf{p}}$ nor $\dot{\mathbf{q}}$ individually, and stability must be analysed for the complete interconnected dynamics.

7. Stability of the controller implementation with DSD reactions
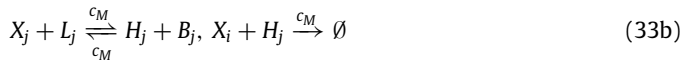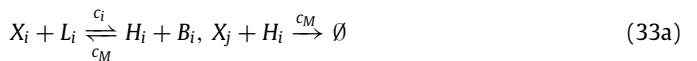
It remains to verify whether the stability properties predicted from analysing the system's CRNs are observed when the closed-loop system is implemented with nucleic acids. The DSD circuitry is verified in *Visual DSD* (Lakin, Youssef, Polo, Emmott, & Phillips, 2011), a rapid prototyping tool for precise analysis of reactions with nucleic acids, via both deterministic and stochastic simulations. Each reaction in (2) is translated to the DSD networks according to Fig. 8 of Yordanov et al. (2014). For the *catalysis* (2a), we use Join/Fork templates (Chen et al., 2013) where

$$\mathbf{X_i} + JoinX_i \overset{c_i}{\underset{c_M}{\rightleftharpoons}} JoinX_i^{-1} + O_{ii} \tag{31a}$$

$$JoinX_i^{-1} + T_i \overset{c_M}{\underset{c_M}{\rightleftharpoons}} JoinX_i^{-2} + O_{ij} \tag{31b}$$

$$JoinX_i^{-2} + J_i \overset{c_M}{\rightarrow} \emptyset \tag{31c}$$

$$O_{ii} + ForkX_i \overset{c_M}{\underset{c_M}{\rightleftharpoons}} ForkX_i^{-1} + \mathbf{X_i} \tag{31d}$$

$$O_{ij} + ForkX_j \overset{c_M}{\underset{c_M}{\rightleftharpoons}} ForkX_j^{-1} + \mathbf{X_j} \tag{31e}$$

$$ForkX_i^{-1} + F_{ij} \overset{c_M}{\rightarrow} \emptyset, \ ForkX_j^{-1} + F_{ij} \overset{c_M}{\rightarrow} \emptyset \tag{31f}$$

The *degradation* reaction from (2b) is set with

$$X_j + G_j \overset{c_j}{\rightarrow} \emptyset \tag{32}$$
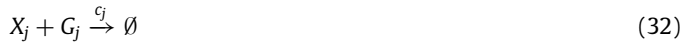
The *annihilation* reaction (2c) is translated into

$$X_i + L_i \overset{c_i}{\underset{c_M}{\rightleftharpoons}} H_i + B_i, \ X_j + H_i \overset{c_M}{\rightarrow} \emptyset \tag{33a}$$

$$X_j + L_j \overset{c_M}{\underset{c_M}{\rightleftharpoons}} H_j + B_j, \ X_i + H_j \overset{c_M}{\rightarrow} \emptyset \tag{33b}$$

The auxiliary species $JoinX_i$, T_i, J_i, $ForkX_i$, $ForkX_j$, F_{ij}, G_j, L_i, B_i, L_j and B_j are all initialised at a large concentration C_{max}, to prevent their consumption from impacting the dynamics significantly (Soloveichik et al., 2010). With the large C_{max} approximation and buffering cancellation discussed in Soloveichik et al. (2010), the unimolecular reaction rates in Example 3 are translated into toehold affinities with: $c_{ki}^{\pm} = 2k_i^{\pm}/C_{max}$, $i \in \{0, 1, 2\}$, and $c_j^{\pm} = 2\gamma_j^{\pm}/C_{max}$, $j \in \{1, \ldots, 8\}$. We set $C_{max} = 10^4$ nM, and with $c_M = 2\eta$ we get the maximum hybridisation rate for full toehold binding of $c_M = 10^6$ (Ms)$^{-1}$ (Zhang et al., 2018). With the nominal symmetrical parameterisation we have in Fig. 6 that p_5 tracks the step inputs of r. After 6×10^4 s, the concentrations converge to the unforced positive equilibrium (Fig. 6), and Fig. 7 shows that concentrations of the auxiliary strands L_j in (33) remain around $C_{max} = 10^4$ nM but are still depleted even if $r^{\pm} = p_j = 0$. With the destabilising parameterisation from Table 3, Fig. 8 shows that the equivalent DSD reactions are also unstable around its equilibrium, emphasising the practical relevance of the stability results.

For a low copy number of molecules, we move away from the assumption of MAK used to represent ODEs with CRNs. More
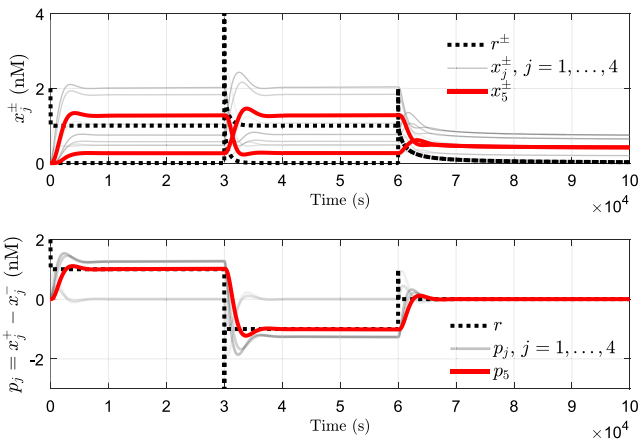
Fig. 6. Simulation in Visual DSD of the DSD reactions (31)–(33) for the symmetrical nominal system, with $\mathbf{x}(0) = 0$ nM and a sequence of steps on $\mathbf{r}$.
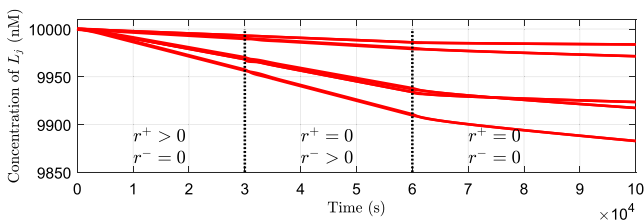

Fig. 7. Concentrations of the auxiliary strands L_j used in (33) for the simulation in Fig. 6. The positive equilibrium of the CRN results in persistent and irreversible consumption, even if the I/O dynamics are at rest for $t > 7 \times 10^4$ s.
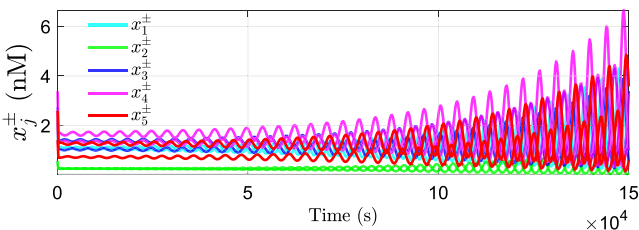

Fig. 8. Simulation in Visual DSD of the DSD network, for the asymmetrical destabilising parameterisation, with $\mathbf{r} = 0$.

work is needed to generalise our results to a stochastic interpretation of the CRN programs, e.g. through analysis using the Linear Noise Approximation of the chemical master equation (Cardelli, Kwiatkowska, & Laurenti, 2016), which scales better to large number of species and reactions. Here, we verify stochastically the results through simulation of the DSD network with Gillespie's algorithm (Gillespie, Hellander, & Petzold, 2013) in Visual DSD, where we see in Fig. 9 the reference tracking behaviour of the nominal system, and in Fig. 10 the unstable departure from equilibrium with the asymmetrical parameterisation of Table 3.

8. Conclusions

Several recent works have applied the dual-rail representation of CRN's to obtain linear I/O models of synthetic feedback control systems, but have not explicitly considered the potential impact of the underlying nonlinear annihilation reactions in their analysis. This new class of IPR derived from CRNs relies on internally nonlinear positive dynamics.

We decomposed the dynamics of the CRN's involved in a typical linear controller design, and highlighted the effects of
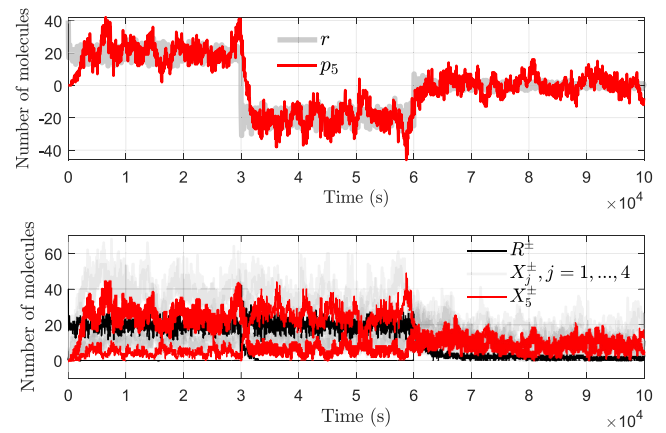

Fig. 9. Stochastic simulations of the DSD network for the nominal parameterisation. With low number of molecules and inherent noise, the I/O dynamics track the reference.
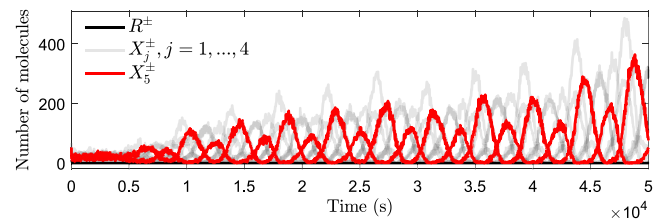

Fig. 10. Stochastic simulations with the destabilising parameterisation result in a divergent output of the DSD network.

the non-observable and nonlinear dynamics − in particular, we showed that the stability of these I/O models does not imply the stability of the underlying chemical network. Under inevitable experimental variability, stability can be affected by the looped interconnection between the nonlinear dynamics arising from biochemical implementation and the linear I/O dynamics resulting from the controller designs. We presented an example of this phenomenon, where the I/O linear system does not capture the instability of the full nonlinear system, and verified this result via simulation of the DSD network that would be implemented experimentally. Our results confirm that the stability of nucleic acid–based controllers must be analysed using the linearisation of the complete nonlinear system, and provide a rigorous theoretical approach for conducting such an analysis.

References

Badelt, Stefan, Shin, Seung Woo, Johnson, Robert F., Dong, Qing, Thachuk, Chris, & Winfree, Erik (2017). A general-purpose CRN-to-DSD compiler with formal verification, optimization, and simulation capabilities. In *International conference on DNA-based computers* (pp. 232–248). Springer.

Blanchini, Franco, El-Samad, Hana, Giordano, Giulia, & Sontag, Eduardo D. (2018). Control-theoretic methods for biological networks. In *2018 IEEE conference on decision and control (CDC)* (pp. 466–483).

Bournez, Olivier, Graça, Daniel S., & Pouly, Amaury (2017). Polynomial time corresponds to solutions of polynomial ordinary differential equations of polynomial length. *Journal of the ACM, 64*(6), 1–76.

Cacace, Filippo, Farina, Lorenzo, Germani, Alfredo, & Manes, Costanzo (2012). Internally positive representation of a class of continuous time systems. *IEEE Transactions on Automatic Control, 57*(12), 3158–3163.

Cardelli, Luca (2013). Two-domain DNA strand displacement. *Mathematical Structures in Computer Science, 23*(2), 247–271.

Cardelli, Luca, Kwiatkowska, Marta, & Laurenti, Luca (2016). Stochastic analysis of chemical reaction networks using linear noise approximation. *Biosystems, 149*, 26–33.

Chatterjee, Gourab, Chen, Yuan-Jyue, & Seelig, Georg (2018). Nucleic acid strand displacement with synthetic mRNA inputs in living mammalian cells. *ACS Synthetic Biology, 7*(12), 2737–2741.

Chen, Yuan-Jyue, Dalchau, Neil, Srinivas, Niranjan, Phillips, Andrew, Cardelli, Luca, Soloveichik, David, et al. (2013). Programmable chemical controllers made from DNA. *Nature Nanotechnology*, 8(10), 755–762.

Chiu, Tai Yin, Chiang, Hui Ju K., Huang, Ruei Yang, Jiang, Jie Hong R., & Fages, François (2015). Synthesizing configurable biochemical implementation of linear systems from their transfer function specifications. *PLoS One*, 10(9), Article e0137442.

Dalchau, Neil, Szép, Gregory, Hernansaiz-Ballesteros, Rosa, Barnes, Chris P., Cardelli, Luca, Phillips, Andrew, et al. (2018). Computing with biological switches and clocks. *Natural Computing*, 17(4), 761–779.

Daniel, Ramiz, Rubens, Jacob R., Sarpeshkar, Rahul, & Lu, Timothy K. (2013). Synthetic analog computation in living cells. *Nature*, 497(7451), 619–623.

De Leenheer, Patrick, & Aeyels, Dirk (2001). Stabilization of positive linear systems. *Systems & Control Letters*, 44(4), 259–271.

Fages, François, Le Guludec, Guillaume, Bournez, Olivier, & Pouly, Amaury (2017). Strong turing completeness of continuous chemical reaction networks and compilation of mixed analog-digital programs. In *International conference on computational methods in systems biology* (pp. 108–127). Springer.

Farina, Lorenzo, & Rinaldi, Sergio (2000). *Positive linear systems: Theory and applications* (p. 305). New York: Wiley.

Gillespie, Daniel T., Hellander, Andreas, & Petzold, Linda R. (2013). Perspective: Stochastic algorithms for chemical kinetics. *The Journal of Chemical Physics*, 138(17), 170901.

Groves, Benjamin, Chen, Yuan Jyue, Zurla, Chiara, Pochekailov, Sergii, Kirschman, Jonathan L., Santangelo, Philip J., et al. (2016). Computing in mammalian cells with nucleic acid strand exchange. *Nature Nanotechnology*, 11(3), 287–294.

Hancock, Edward J., & Ang, Jordan (2019). Frequency domain properties and fundamental limits of buffer-feedback regulation in biochemical systems. *Automatica*, 103, 330–336.

Jeong, Dohyun, Klocke, Melissa, Agarwal, Siddharth, Kim, Jeongwon, Choi, Seungdo, Franco, Elisa, et al. (2019). Cell-free synthetic biology platform for engineering synthetic biological circuits and systems. *Methods and Protocols*, 2(2), 39.

Khalil, Hassan (2015). *Nonlinear control, global edition*. Essex, England: Pearson Education Limited.

Koch, Mathilde, Faulon, Jean-Loup, & Borkowski, Olivier (2018). Models for cell-free synthetic biology: make prototyping easier, better, and faster. *Frontiers in Bioengineering and Biotechnology*, 6, 182.

Kokotovic, Petar, Khalil, Hassan K., & O'Reilly, John (1999). *Singular perturbation methods in control: Analysis and design, Vol. 25*. Siam.

Lakin, Matthew R., Youssef, Simon, Polo, Filippo, Emmott, Stephen, & Phillips, Andrew (2011). Visual DSD: a design and analysis tool for DNA strand displacement systems. *Bioinformatics*, 27(22), 3211–3213.

Oishi, Kevin, & Klavins, Eric (2011). Biomolecular implementation of linear I/O systems. *IET Systems Biology*, 5(4), 252–260.

Paulino, Nuno M. G., Foo, Mathias, Kim, Jongmin, & Bates, Declan G. (2019a). PID and state feedback controllers using DNA strand displacement reactions. *IEEE Control Systems Letters*, 3(4), 805–810.

Paulino, Nuno M. G., Foo, Mathias, Kim, Jongmin, & Bates, Declan G. (2019b). Robustness analysis of a nucleic acid controller for a dynamic biomolecular process using the structured singular value. *Journal of Process Control*, 78C, 34–44.

Roszak, Bartek, & Davison, Edward J. (2009). Necessary and sufficient conditions for stabilizability of positive LTI systems. *Systems & Control Letters*, 58(7), 474–481.

Sawlekar, Rucha, Montefusco, Francesco, Kulkarni, Vishwesh V., & Bates, Declan G. (2016). Implementing nonlinear feedback controllers using DNA strand displacement reactions. *IEEE Transactions on NanoBioscience*, 15(5), 443–454.

Siami, Milad, Motee, Nader, Buzi, Gentian, Bamieh, Bassam, Khammash, Mustafa H., & Doyle, John C. (2020). Fundamental limits and tradeoffs in autocatalytic pathways. *IEEE Transactions on Automatic Control*, 65(2), 733–740.

Soloveichik, David, Seelig, Georg, & Winfree, Erik (2010). DNA as a universal substrate for chemical kinetics. *Proceedings of National Academy of Sciences, USA*, 107(12), 5393–5398.

Song, Tianqi, Garg, Sudhanshu, Mokhtar, Reem, Bui, Hieu, & Reif, John (2016). Analog computation by DNA strand displacement circuits. *ACS Synthetic Biology*, 5(8), 898–912.

Srinivas, Niranjan, Parkin, James, Seelig, Georg, Winfree, Erik, & Soloveichik, David (2017). Enzyme-free nucleic acid dynamical systems. *Science*, 358(6369), eaal2052.

Tóth, Peter, & Érdi, János (1989). *Mathematical models of chemical reactions: Theory and applications of deterministic and stochastic models*. Manchester University Press.

Vasić, Marko, Soloveichik, David, & Khurshid, Sarfraz (2020). CRN++: Molecular programming language. *Natural Computing*, 1–17.
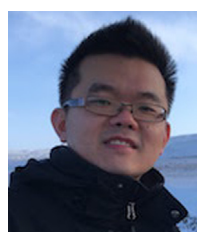
Yordanov, Boyan, Kim, Jongmin, Petersen, Rasmus L., Shudy, Angelina, Kulkarni, Vishwesh V., & Phillips, Andrew (2014). Computational design of nucleic acid feedback control circuits. *ACS Synthetic Biology*, 3(8), 600–616.

Zhang, Jinny X., Fang, John Z., Duan, Wei, Wu, Lucia R., Zhang, Angela W., Dalchau, Neil, et al. (2018). Predicting DNA hybridization kinetics from sequence. *Nature Chemistry*, 10(1), 91–98.

Zou, Chengye, Wei, Xiaopeng, Zhang, Qiang, Liu, Chanjuan, Zhou, Changjun, & Liu, Yuan (2017). Four-analog computation based on DNA strand displacement. *ACS Omega*, 2(8), 4143–4160.

Nuno Miguel Gomes Paulino received his B.Sc. degree in Electronic Engineering and Computer Science in 2002, and M.Sc. degree in Decision Systems and Control in 2005, both from the Instituto Superior Técnico, Portugal. In 2006 he started a two-year training fellowship at the European Space Agency, then followed by 8 years in industry, working in research projects for guidance, control and navigation for aerospace applications. In 2016 he enrolled in the EPSRC/BBSRC Oxford-Warwick-Bristol Centre for Doctoral Training in Synthetic Biology, and he is currently completing his PhD at the University of Warwick. His research is focussed on the application of systems and control theory to the design of DNA systems.

Mathias Foo received the BEng (Hons.) and MEngSc degrees in electronic engineering from Multimedia University, Malaysia, in 2002 and 2004, respectively, and the PhD degree from the University of Melbourne, Melbourne, Australia, in 2012. He was a post-doctoral research fellow with the Asia Pacific Center for Theoretical Physics (APCTP), Pohang, South Korea, from 2012–2015 and was a research fellow in the Warwick Integrative Synthetic Biology Centre, School of Engineering, University of Warwick, UK from 2015–2018. He is currently a Lecturer in the School of Mechanical, Aerospace and Automotive Engineering, Coventry University, UK and an Honorary Research Fellow at the University of Warwick, UK. His research interests include dynamical system modelling, application of control system, and control theory for systems and synthetic biology.

Jongmin Kim received the B.S. degree in Life Sciences from Pohang University of Science and Technology in 2000 and Ph.D. degree in Biology from California Institute of Technology in 2007. After completing post-doctoral training at California Institute of Technology and Harvard University, he was appointed as an assistant professor at Pohang University of Science and Technology in 2018. He has focused on the synthetic biology of microorganisms; particularly, he has contributed to the construction of complex logic circuits using riboregulators in microorganisms. His research group is highly interested in the determination of design principles of riboregulators in bacteria and other organisms, which could be utilised for novel synthetic regulatory circuits.

Declan G. Bates received the B.Eng and Ph.D. degrees in Electronic Engineering from Dublin City University in 1992 and 1996 respectively, after which he joined the Control and Instrumentation Research Group led by Prof. Ian Postlethwaite in the Department of Engineering at Leicester University. At Leicester, he worked as a PDRA, lecturer, and senior lecturer, before being awarded a Personal Chair in Control Engineering. In 2010, he was appointed Professor of Biological Systems Engineering at the University of Exeter, and in 2013 he moved to the University of Warwick as Professor of Bioengineering. His research is focussed on the modelling, simulation, analysis and control of biological and medical systems. He is the co-author of "Feedback Control in Systems Biology", published by Taylor & Francis.